A multi-level porous MgO/biochar composite for the highly efficient adsorption of Pb(II) and Cd(II) from water

Zhang Guojie[1,2], Liu Shiwei[1,2], Sun Qihua[1,3], Sun Jun[1,3], Tian Ning[1,2,*], Wu Zhaofeng[1,2,*], Jiang Li[4,*]

(1. *School of Materials Science and Engineering*, *Xinjiang University*, *Urumqi*, *Xinjiang* 830046, *China*;
2. *Xinjiang Key Laboratory of Solid State Physics and Devices*, *Urumqi*, *Xinjiang* 830046, *China*;
3. *School of Physics Science and Technology*, *Xinjiang University*, *Urumqi*, *Xinjiang* 830046, *China*;
4. *State Key Laboratory of Desert and Oasis Ecology*, *Xinjiang Institute of Ecology and Geography*, *Chinese Academy of Sciences*, *Urumqi* 830011, *China*)

Abstract: A MgO/biochar composite (MBC) with a wide range of pore sizes was prepared by a $MgCl_2$-NaOH co-impregnation method using lavender stalks as the biochar source, which can effectively remove Pb(II) and Cd(II) from wastewater. The co-impregnation treatment resulted in a specific surface area of the MBC that was approximately 54 times greater than that of the biochar derived from untreated stalks. The ion-exchange capacity of MBC was increased by the incorporation of MgO nanoparticles, which increased the alkali metal ion (Mg^{2+}) content. These specific structures and compositions gave the MBC a high adsorption capacity for Pb(II) and Cd(II). The adsorption data followed a quasi second-order kinetic model. For Cd(II) and Pb(II), the maximum adsorption capacities of MBC-700 (treated at 700 ℃ for 2 h) reached 520 mg/g and 808 mg/g, respectively. The primary adsorption mechanisms were ion exchange, precipitation, electrostatic attraction and surface complexation. Furthermore, metallic lead was recovered by using the reducing properties of the biochar at high temperatures. This study provides a reference for developing inexpensive and efficient heavy metal adsorbents and the low-carbonization utilization of biomass waste.

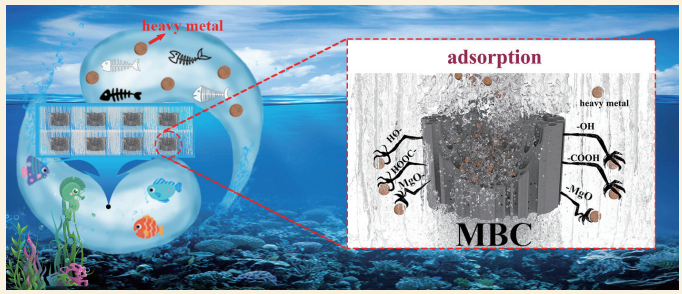

Key words: MgO/biochar composite; Multi-level pore; Pb(II) absorption; Cd(II) absorption; adsorption mechanism

1 Introduction

In recent years, the rapid growth of global economy and population has led to expanding industrialization, causing the problem of heavy metal pollution to become increasingly serious. An increasing quantity of heavy metals is flowing into the water bodies on which human beings depend, resulting in many rivers and groundwater reserves with heavy metal levels exceeding safety standards[1−2]. Heavy metal ions are characterized by their stability and persistence, as they cannot be degraded or destroyed in nature. They can enter the human body through the food chain, thus posing a serious threat to human health. Among these heavy metal ions, lead (Pb(II)) and cadmium (Cd(II)) are not only categorized as human carcinogens, but are also the most common contaminants in many industrial applications[3]. The presence of excess cadmium in water or food ingested by the human body increases the likelihood of developing diabetes and kidney disease. Similarly, excessive exposure to and absorption of Pb(II) by human body can result in chronic poisoning, with Pb(II) damaging the body's central nervous system, kidneys and hematopoietic system, as well as the digestive system, ultimately leading to death[4]. Therefore, developing cost-effective ways to remove Pb(II) and cadmium from wastewater or contaminated surface water is essential for pollution con-

Received: November 16, 2025
Revised: February 25, 2026
Accepted: February 26, 2026

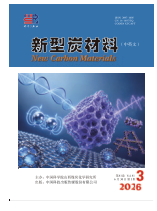

trol and environmental remediation.

Currently, the main treatment methods for removing heavy metals from contaminated waters are chemical precipitation, electrochemical and redox methods, ion exchange, solvent extraction, adsorption and membrane separation. Among these techniques, the adsorption method is widely used for the removal of heavy metal ions due to its simple operation, high removal rate, low cost of raw materials and adaptability to various environments[5]. Many adsorbents have been reported for the removal of heavy metals by adsorption, such as activated carbon[6], g-C_3N_4[7], and graphene oxide[8]. However, most of these materials have low removal rates of heavy metal ions and are expensive and can cause secondary pollution to the environment. Therefore, there is an urgent need to explore novel materials to remove heavy metals from wastewater.

Biochar is a carbon-rich solid material with well-developed porosity, surface functional groups, and also various minerals[9]. In recent decades, agricultural and forestry wastes have been widely used as precursors for the preparation of adsorbents for biochar materials due to their low cost and easy accessibility. Biochar adsorbents derived from agroforestry wastes are a low-cost and sustainable approach for the removal of heavy metals from water pollution. However, the adsorption capacity of biochar for heavy metal ions is often limited by its pore structure, specific surface area and surface properties, necessitating modification methods to enhance its adsorption capacity[10]. Common methods of modifying biochar include steam treatment, ball milling, acid treatment, alkaline treatment, metal oxide treatment and treatment with organic compounds[11−12]. Among these methods, leveraging the ion exchange and mineralization properties of metal oxides has been shown to be an effective strategy to significantly improve the adsorption capacity of biochar[13−15]. However, when using metal oxides for modification, it is also necessary to consider their potential for secondary environmental pollution and the ease of sourcing raw materials. For instance, in biochar modified with MnO, manganese may undergo reductive dissolution into mobile ions like Mn^{2+} under acidic or reducing conditions. Among various metal oxides, MgO is considered a promising candidate for modification owing to its abundant reserves and low toxicity[16]. Previous studies on MgO-modified biochar have mainly explored its combination with various biomass precursors, for instance, banana peel[17] and corn stalk[18]. However, the use of a single metal oxide modification (MgO modification) has some limitations because this method does not improve the physical structure of the biochar well. Single MgO-modified biochar primarily relies on the inherent pores of biomass, with MgO potentially clogging these channels. In some cases, single metal oxide modification can even reduce biochar's specific surface area, which limits its adsorption capacity for heavy metals[19−20]. While using metal oxide modification, adding alkaline activator can decompose lignocellulose in biomass and corrode biochar, which can achieve the effect of expanding the specific surface area of biochar and improving the pore structure of biochar, providing more sites for the adsorption of heavy metal ions [21−22].

In the Ili Valley region of Xinjiang, China, the annual production of lavender essential oil and dried flowers is nearly 1.5×10^5 kg, generating a large amount of discarded lavender straw, which is not only a waste of resources but also pollutes the environment. Lavender straw has been reported in construction and agricultural feed, but there is no literature report on the application of lavender straw-based biochar for the removal of heavy metals from wastewater. Therefore, in this work, we report a novel magnesium-alkali modified biochar from lavender straw for the removal of Cd(II) and Pb(II) from water. The effects of different factors including pH, initial concentration, contact time and ionic strength on the adsorption of Cd(II) and Pb(II) by this magnesium-alkali modified biochar material were systematically investigated through batch adsorption experiments. Combined with the adsorption experimental data and various characterization results, the adsorption mechanisms of Cd(II) and Pb(II) were derived. This study

not only provides a new perspective for the removal of heavy metals, but also reveals the potential application of magnesium-alkali modified biochar composites in pollution control.

2 Experimental

2.1 Materials

Lavender straw was produced from Yili, Xinjiang, China. $MgCl_2·6H_2O$ (≥99%) was purchased from Tianjin Xinbote Chemical Co., Ltd. (Tianjin, China). NaOH (≥96%) was purchased from Tianjin Beilian Fine Chemicals Development Co., Ltd. (Tianjin, China). $CdCl_2·2.5H_2O$ (≥99%) was purchased from Tianjin Bodi Chemical Co., Ltd. (Tianjin, China). $Pb(NO_3)_2$ (AR) was purchased from Sinopharm Chemical Reagent Co., Ltd. (Shanghai, China). Deionized water was used for the preparation of all solutions.

2.2 Preparation of MgO-biochar composite

A certain amount of waste lavender straw was cut into a 2-3 cm, washed with deionized water to remove surface impurities, and dried at 60 °C for 12 h. To prepare a 0.8 mol/L $MgCl_2$ solution, 10 g of dried lavender straw was weighed and added to the configured $MgCl_2$ solution and the mixture was stirred in a magnetic stirrer for 1 h at 400 r/min. Then the pH value of the mixture solution was adjusted to 10-11 with 5 mol/L NaOH solution and stirred for 2 h at 500 r/min. The filtered and separated mixture was dried at 60 °C for 12 h. The dried mixture was divided into 4 portions and placed into a chemical vapor deposition furnace and carbonized at 500, 600, 700 and 800 °C for 2 h (under N_2 protection at a heating rate of 5 °C/min), respectively. The carbonized samples were named MBC-500, MBC-600, MBC-700 and MBC-800, respectively. All samples were rinsed with deionized water, dried, then crushed and stored in a desiccator for further experiments. The raw lavender straw biochar carbonized at 700 °C was named BC. A schematic diagram of the sample preparation is shown in Fig. 1.

The obtained sample (MBC-700) showed the best adsorption performance for Cd(II) and Pb(II) (Fig. S1).

2.3 Characterization

The surface morphologies of samples were ob-

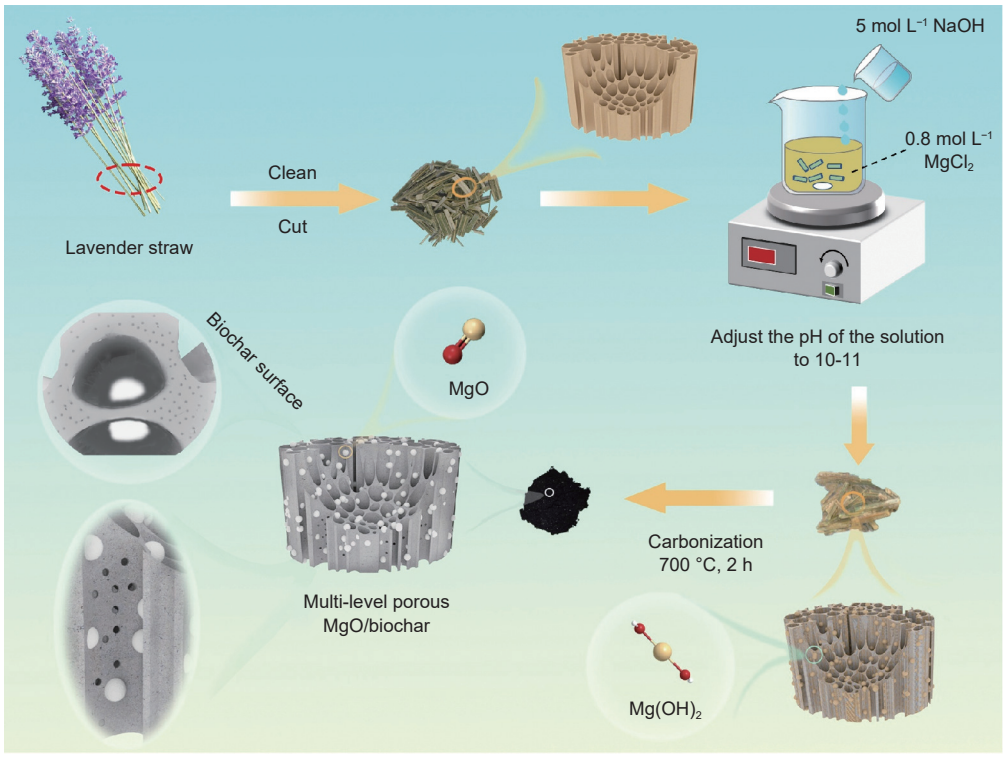

Fig. 1 Preparation diagram of multi-level porous MgO/biochar composite

tained by scanning electron microscopy (SEM, Zeiss, Sigma300, Germany), together with an X-ray energy spectrometer (EDS, Oxford Instruments, Xplore 30, Britain) to analyze the chemical composition of the sample surfaces. The morphology of samples were characterized by transmission electron microscopy (TEM, JEOL, JEM 2100 F, Japan). The crystal structure of the samples was analyzed by X-ray diffraction (XRD, BRUKER, D8 Advance, Germany). The Brunauer-Emmett-Teller (BET) surface area was determined by determining the N_2 adsorption-desorption isotherm using a porosity analyzer (micromeritics, ASAP2460, USA) to measurements. Changes in the functional groups of the samples were determined by Fourier Transform Infrared Spectroscopy (FTIR, Thermo, Thermo Nicolet iS5, USA) with a resolution of 2.0 cm^{-1} and a range of 400–4000 cm^{-1}. The samples were analyzed using a light ray photoelectron spectrometer (XPS, Thermo Fisher Scientific K-Alpha, USA) to analyze the elemental composition and elemental species of the samples. In addition, in all adsorption experiments, the content of heavy metals in solution was determined using inductively coupled plasma emission spectrometry (ICP-OES, Perkin Elmer, Optima 8000, USA).

2.4 Batch adsorption experiments

Dissolve a suitable amount of $CdCl_2·2.5H_2O$ or $Pb(NO_3)_2$ solid in deionized water to prepare a stock solution, further dilute accordingly to prepare a 20 mL solution of heavy metal at the required concentration. The adsorption experiment involves adding a certain amount of adsorbent to a series of conical flasks containing heavy metal solutions, then carrying out the experiment in a constant temperature oscillating box at 25 ± 1 °C and an oscillation frequency of 160 r/min. If not specified, the initial pH of all heavy metal solutions used for the adsorption experiment is adjusted to 5.0 ± 0.1, aiming to simulate the real aqueous environment, and at this pH, experimental errors caused by the precipitation of Cd(II) and Pb(II) can be avoided. The adjusting solutions used are 0.1 mol/L HCl or 0.1 mol/L NaOH. By systematically changing the solution pH (2–6), Na^+ ion strength (0–200 mmol/L), and humic acid content (0–50 mg/L), the influence of environmental conditions on the adsorption of heavy metal ions by the adsorbent is examined. After the adsorption experiment, filter the samples through a 0.22 μm filter membrane and measure the concentration of Cd(II) or Pb(II) in the solution. The adsorption capacity q_t (mg/g) of biochar for Cd(II) or Pb(II) in the solution at time t (min) is calculated using Eq. (1), and the removal efficiency η (%) is calculated using Eq. (2).

$$q_t = \frac{(C_0 - C_t) \times V}{m} \tag{1}$$

$$\eta = \frac{C_0 - C_t}{C_0} \times 100\% \tag{2}$$

Where C_0 (mg/L) is the initial concentration of heavy metal ions in the solution, C_t (mg/L) is the concentration of heavy metal ions in the solution at time t (min), V (mL) is the volume of the solution, and m (g) is the mass of adsorbent added.

Chapter 1 of the Supporting Material provides a detailed overview of the specific procedures for the adsorption kinetic studies and adsorption isotherms experiments.

3 Results and discussion

3.1 Physicochemical properties

The morphology of BC and MBC-700 was characterized by SEM (Fig. 2). The carbonized lavender straw retained the tubular structure (Fig. 2a) and showed a smooth surface (Fig. 2b). Meanwhile, some porosity was observed in the tube wall (Fig. 2c). In contrast, the magnesium-alkali modified MBC-700 samples also retained the tubular structure, but the surface became rougher and a large number of pores appeared (Fig. 2e-f). This might be attributed to NaOH promoting the decomposition of organic matter in lavender straw, which reorganizes the solid matrix to form a developed porous structure, and NaOH also etches the surface of the biochar during pyrolysis and forms mesopores. This mesoporous structure can provide more adsorption sites for heavy metals[23].

The SEM characterization results indicate that MBC-700 would be an effective adsorbent. Elemental analysis of the selected area of Fig. 2g was carried out

using EDS, which showed that the composition mainly consisted of C, O and Mg (Fig. 2h-j). The atomic percentages of the three elements are listed in Fig. S2. The elements of Mg and O are uniformly distributed on the surface and in the pores of the MBC-700, indicating successful loading of MgO onto both the surface and pores of the MBC-700 samples. To obtain a deeper understanding of the structure of the MBC-700 composite, the TEM images were further investigated (Fig. 2k-l). Fig. 2k shows the fragments of MBC-700 and a large number of lattice fringes can be seen in the higher magnification images of the MBC-700. Fig. 2l shows the lattice stripe spacing of 0.21, 0.15 and 0.24 nm corresponding to the (2 0 0), (2 2 0) and (1 1 1) crystal faces of MgO, respectively[24−25].

A disordered carbon structure at the edge of the MgO also can be seen in Fig.2l, indicated by the red dashed line. This structure is attributed to the lavender straw biochar. Plant straw contains many vertical and hollow tubes that act as high-speed pathways for plants to transport water and nutrients. As shown above, MBC-700 maintains this structure, and the abundant hydroxyl groups and mesopores in plant straw can effectively adsorb and disperse heavy metal ions. In conclusion, a reasonable modification endowed MBC-700 with a high specific surface area, abundant exposed active sites, fast mass transfer pathways and a large number of mesopores, which may result in rapid heavy metal ion permeation/diffusion

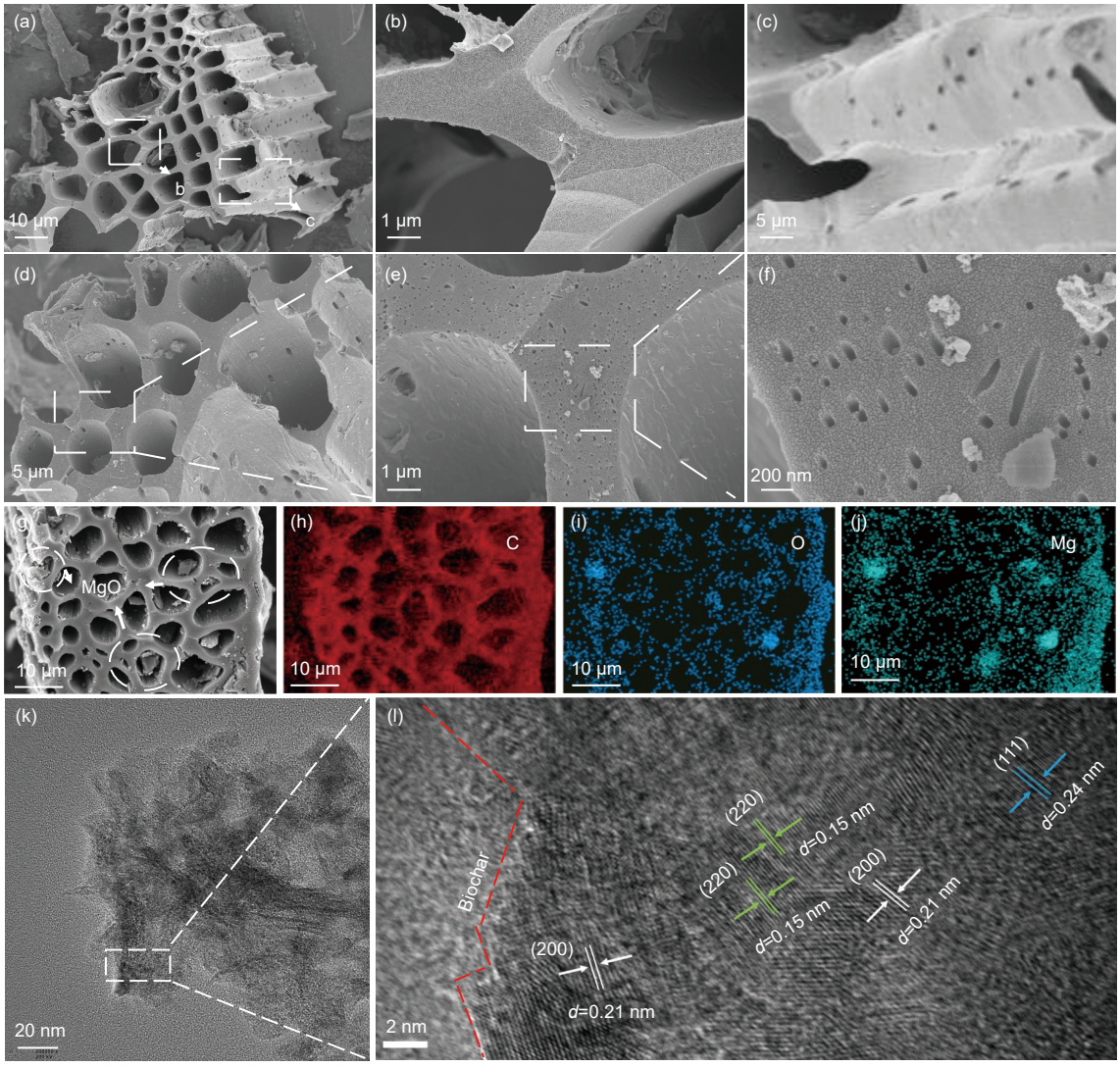

Fig. 2 (a-c) SEM images of BC. (d-f) SEM images of MBC-700. (g-j) Elemental distribution of MBC-700. (k-l) TEM images of MBC-700

and accelerated adsorption of heavy metal ions[26]. In addition, successful loading of MgO can increase the alkali metal ion (Mg^{2+}) content of the MBC-700 and thus enhance the ion exchange capacity of the MBC-700[27].

The structure of the samples was further analyzed using XRD and the results are shown in Fig. 3a. The broad diffraction peak at 24° is assigned to the biochar matrix derived from the carbonization of lavender straw. Relative to the pristine BC, the modified samples exhibit five new diffraction peaks at 2θ values of 36.9°, 42.9°, 62.3°, 74.7° and 78.7°, which correspond to the (111), (200), (220), (311) and (222) crystal planes of MgO, respectively (JCPDS Card No. 45-0946), confirming the successful loading of MgO onto the biochar[28].

Both BC and MBC-700 exhibit the common IR characteristic peaks of straw-derived lignin. They are shown in Fig. 3b. The telescopic vibration of O—H groups is located at around 3431 cm^{-1}[29]. The enhanced O—H vibration peak on MBC-700 compared with BC indicates that the relative content of O—H groups on biochar can be increased after magnesium alkali modification, and more oxygen-containing functional groups are more favorable for the adsorption of heavy metals[30]. The absorption peak at 2927 cm^{-1} is attributed to the stretching vibration of C—H bonds in cellulose and hemicellulose[31]. The peak observed around 1703 cm^{-1} corresponds to the stretching vibration of the C=O bond[32]. For both BC and MBC-700, the peak near 1595 cm^{-1} is associated with C=C stretching vibration in the aromatic skeleton of lignin[33]. Meanwhile, the vibrational peak at 1423 cm^{-1} on BC and MBC-700 is assigned to the O—C=O stretching vibration in carboxylate group[34]. The absorption peak at 1040 cm^{-1} is attributed to the C—O stretching vibration in the sample BC. Following surface modification, the peak position of the C—O peak undergoes a red shift, moving to the vicinity of 1097 cm^{-1} in MBC-700 [35]. Meanwhile, after the modification, a new absorption peak appears at 567 cm^{-1} on sample MBC-700, which may

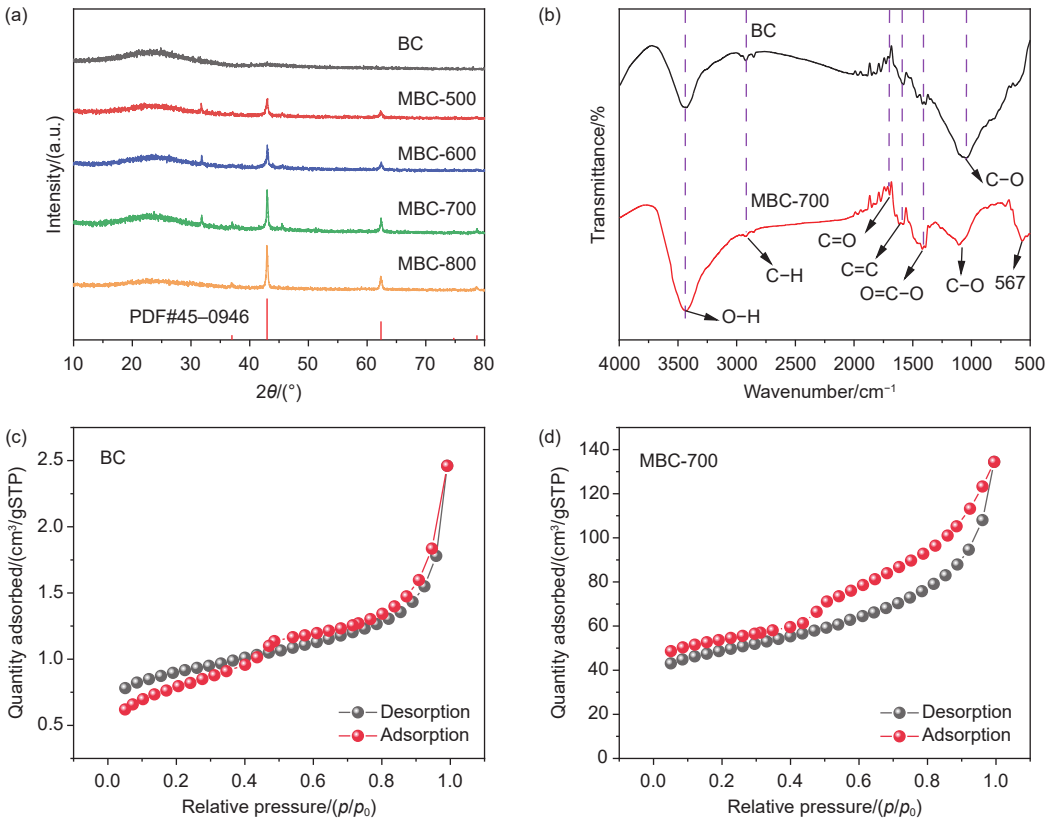

Fig. 3 (a) XRD patterns of BC, MBC-500, MBC-600, MBC-700 and MBC-800. (b) FT-IR spectra of BC and MBC-700. (c) N_2 adsorption/desorption isotherms of BC and (d) MBC-700

be due to the formation of Mg—O metal bonds[36].

The specific surface area and pore structure of the samples were further analyzed using BET, the results of which are shown in Fig. 3c, d and Table S1. Compared with the original biochar BC, the specific surface area of MBC-700 sample increased from 3 to 158 m^2/g (Fig. 3c-d), which is approximately 54 times higher. The increase in the specific surface area may be related to the loading of MgO and modification of NaOH. The MgO particles are polycrystalline and porous, and this morphology will allow the modified MgO-loaded particles of the biochar to have a higher specific surface area. The pore structure produced by NaOH etching of the biochar surface also contributes significantly to the increase in specific surface area[37−38]. The total pore volume increased from 0.003 to 0.139 cm^3/g, which is approximately 42 times higher, and the increase of pore volume can enable the biochar to adsorb and store more heavy metals in the pores, thus increasing its own adsorption capacity[39]. The pore size distribution graph shows that MBC-700 has predominantly mesoporous pores in the 3-6 nm range (Fig. S3). According to the data in Table S1, the average pore sizes of MBC-700 and BC are 6.971 and 7.345 nm, respectively. The decrease in the average pore size after modification may be due to the Mg compounds entering and clogging the biochar pores[40]. Additionally, the hydrated radius of Pb^{2+} is relatively small (~ 0.401 nm), with high charge density and strong polarizability. This allows Pb^{2+} to penetrate deeply into the micropores of the tube walls, where it can closely interact with oxygen-containing functional groups (—COOH,—OH) or MgO sites, promoting complexation and fully utilizing the high specific surface area regions. In contrast, Cd^{2+} has a larger hydrated radius (~ 0.426 nm) and relatively lower charge density, resulting in limited accessibility to micropores. It relies more on mesopores and macropores for transport, with the tube cavities and larger mesopores serving as the primary sites for its adsorption[41].

3.2 Adsorption characteristics

In order to explore the potential adsorption mechanism, the adsorption kinetic model and adsorption isotherm model were chosen to analyze the adsorption process of Cd(II) and Pb(II) on MBC-700 and BC at the same temperature. Fig. 4 shows the relationship between the adsorption capacity and adsorption time of MBC-700 and BC in the adsorption of Cd(II) and Pb(II), MBC-700 has the fastest adsorption rate of Cd(II) and Pb(II) in 0-320 min.

After the adsorption time exceeds this range, the adsorption rate of MBC-700 for Cd(II) and Pb(II) decreases with the gradual decrease of the effective adsorption sites on MBC-700. MBC-700 reached equilibrium in the adsorption process with the adsorption of Cd(II) and Pb(II) of 520 and 781 mg/g, respectively. For BC, the adsorption process basically reached equilibrium at 120 min, and the adsorption amounts of Cd(II) and Pb(II) are 50 and 92 mg/g, respectively (Fig. 4c-d). The adsorption amounts of Cd(II) and Pb(II) at equilibrium by MBC-700 were 8-9 times higher than those of BC, which showed excellent adsorption capacity. These results can be attributed to the fact that the specific surface area of MBC-700 is much larger than that of BC and possesses abundant MgO loadings, which provide many new adsorption sites for Cd(II) and Pb(II) adsorption. The adsorption data were further fitted with pseudo-first-order kinetic model (Fig. 4a-b), and the corresponding fitting parameters are listed in Table S2. The pseudo-second-order kinetic model demonstrated a better correlation with the original data (R^2 values closer to 1), suggesting that chemisorption may be the main adsorption mechanism[42].

Langmuir and Freundlich models were used to characterize the equilibrium adsorption data for MBC-700 and BC (Fig. 5). The fitting data about the 2 models are shown in Table S3. In this study, the adsorption isotherms of Cd(II) or Pb(II) on MBC-700 could not be adequately described by the classical Langmuir and Freundlich models. Specifically, the actual adsorption capacity had already reached its limit, yet the fitted curves did not exhibit a clear plateau. This suggests that the adsorption process is not a simple monolayer adsorption. Through analysis, we believe

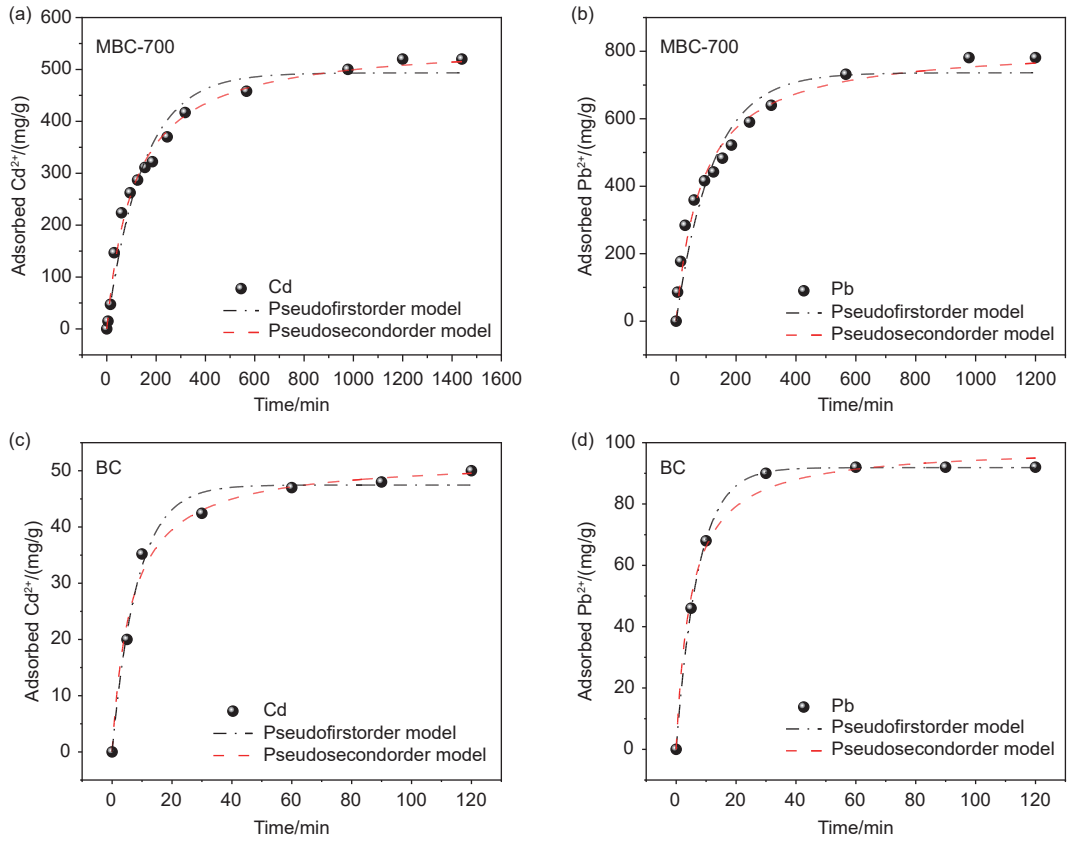

Fig. 4 (a-b) Adsorption kinetics of Cd(II) and Pb(II) adsorption by MBC-700. (c-d) Adsorption kinetics of Cd(II) and Pb(II) adsorption by BC (Adsorbent dose=0.5 g/L, pH=5.0±0.1)

this is likely due to the fact that the adsorption of Cd(II) or Pb(II) onto MBC-700 is not governed by a single mechanism. For example, after modification, the adsorbent surface becomes alkaline, and during adsorption, Cd(II) or Pb(II) can form hydroxide precipitates with OH^- on the adsorbent surface. Precipitation is a bulk-phase process rather than a surface monolayer adsorption. Moreover, besides precipitation, the adsorption of Cd(II) or Pb(II) may involve significant ion exchange (with Mg^{2+} in MBC-700), which complicates the adsorption stoichiometry. Given these potential combined mechanisms, forcing the use of simplified single-parameter models (such as Langmuir) to fit the data may yield a theoretically derived "maximum adsorption capacity" (Q_{max}) that lacks physical accuracy and could obscure the true adsorption behavior. Therefore, instead of forcibly applying the Langmuir and Freundlich models to calculate a theoretical Q_{max}, this study focuses on reporting the experimentally observed maximum adsorption amount (the actual adsorption achieved at the highest equilibrium concentration tested). This value is considered more meaningful for evaluating the material's potential in practical applications. For Cd(II) and Pb(II), the Q_{max} of MBC-700 reached 520 and 808 mg/g, respectively.

Under experimental conditions that simulate an actual water volume of 20 mL, the MBC-700 can remove up to 99% of Cd(II) or Pb(II) solutions at low concentrations (0-100 mg/L). And 300 μg/L of Cd(II) or Pb(II) can be purified to far below 10 μg/L using only 0.5 g/L MBC-700 (Table S4). The adsorption of Cd(II) and Pb(II) by MBC-700 in a certain range became larger as the initial concentration of Cd(II) and Pb(II) increased (Fig. 5a-b), while the adsorption of BC for Cd(II) or Pb(II) is lower than that of MBC-700 at different concentrations (Fig. 5c-d).

The MBC-700 sample is compared with the literature of other researchers on adsorption of Cd(II) and Pb(II) and the results are shown in Table 1. The performance of MBC-700 is significantly better than that of these adsorbents, which is attributed to MBC-700

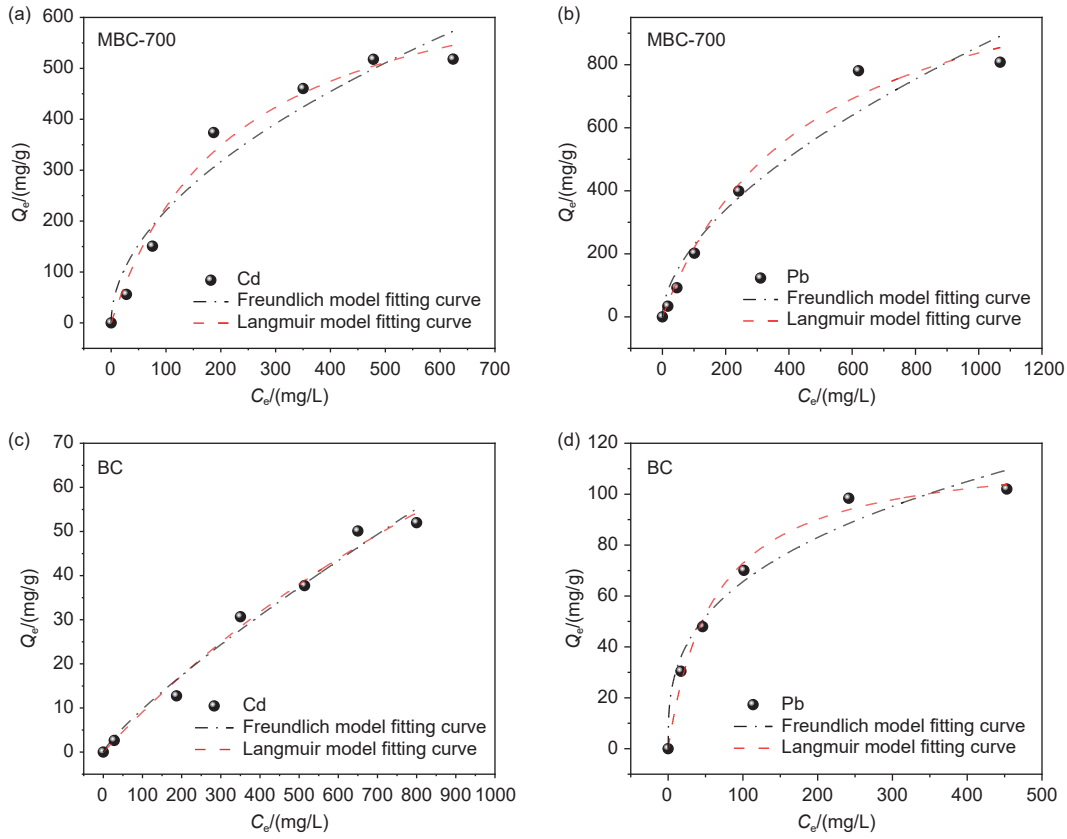

Fig. 5 (a-b) Adsorption isotherms of Cd(II) and Pb(II) adsorbed by MBC-700. (c-d) Adsorption isotherms of Cd(II) and Pb(II) adsorbed by BC. (Adsorbent dose=0.5 g/L, pH=5.0±0.1)

through NaOH etching during the modification process, more adsorption sites were created, and the strong affinity of MgO for Cd(II) and Pb(II). Considering the excellent performance of MBC-700 for Cd(II) and Pb(II) adsorption, it is further investigated.

3.3 Solution chemistry

3.3.1 Effect of initial pH value

In the real environmental adsorption process, the adsorption capacity of the adsorbent will be affected by many environmental factors, among which the pH value of the solution is an important factor to evaluate the adsorption performance of the adsorbent. The adsorption capacity of MBC-700 samples was investigated in the pH range of 2-6. As shown in Fig. 6a, the adsorption of Cd(II) by MBC-700 was limited at pH=2, and the adsorption capacity and removal rate were enhanced with increasing pH in the pH range of 3-6, reaching a maximum at pH=6, with the removal rate of about 60%. The adsorption of Pb(II) by MBC-700 was similarly inhibited at low pH (<2.0), which was significantly enhanced at pH=3 and essentially saturated at pH=4, with the removal rate approaching 90%. The removal rate of Pb(II) by MBC-700 remained essentially unchanged upon further increase in the pH of the initial solution to 6 (Fig. 6b). At lower pH (<2.0), the large amount of H^+ in the solution may have electrostatic repulsion with Cd(II) and Pb(II), which is unfavorable to the adsorption of heavy metal cations by alkali metal biochar[50]. Increasing the pH of the solution ionizes the chemical groups present on the surface of the MBC-700, implying deprotonation. This causes the surface of the MBC-700 to be charged, and the degree of deprotonation of the MBC-700 becomes stronger at increasing pH, and the potential of the surface with a negative charge increases, which is more conducive to the coordination of the heavy metal cations in the solution[51]. It can be seen that MBC-700 can show good adsorption performance for Cd(II) and Pb(II) in a wide pH range (3-6).

3.3.2 Effect of ionic strength

The removal rates of Cd(II) and Pb(II) by MBC-700 at various concentrations are shown in Fig. 6c.

Table 1 Comparison of Cd(II) and Pb(II) removal using different adsorbents based on biochar

Metal	Adsorbent	C_0 (mg/L)	q_{max} (mg/g)	Ref.
Cd(II)	Fe-Mn binary oxide biochar	0-200	141 (pH 5.0)	[43]
	Fe/Ni-biochar	100-180	242 (pH 6.0)	[44]
	Red mud modified bean-worm skin biochar	0-140	74 (pH 7.5)	[45]
	MnO_x modified biochar	10-200	34 (pH 5.0)	[46]
	KOH modified biochar	0.1-20	22 (pH 5.0)	[47]
	MBC-700	0-1000	520 (pH 5.0)	This work
Pb(II)	Fe/Ni-biochar	100-180	217 (pH 6.0)	[44]
	MnOx modified biochar	50-1000	165 (pH 5.0)	[46]
	KOH modified biochar	1-1000	120 (pH 5.0)	[47]
	$KMnO_4$-NaOH modified biochar	0-150	200 (pH 5.0)	[48]
	Zn/Fe modified biochar	60-140	200 (pH 5.0)	[49]
	MBC-700	0-1200	808 (pH 5.0)	This work

The removal of Cd(II) by MBC-700 is almost constant at low Na^+ concentration, and decreased slightly when the concentration is gradually increased to 200 mmol/L. The experimental results show that the removal of Pb(II) by MBC-700 hardly varied with Na^+ concentration. Generally, the increase of ionic strength not only affects the electrostatic attraction between adsorbent and adsorbate but also enhances the hydrophobicity. However, it does not affect the inner surface complexation. In other words, there is no water molecule when the inner surface complex is formed between Cd(II) or Pb(II) and the functional groups on MBC-700. This suggests that the effect of MBC-700 on Cd(II) and Pb(II) by MBC-700 can be

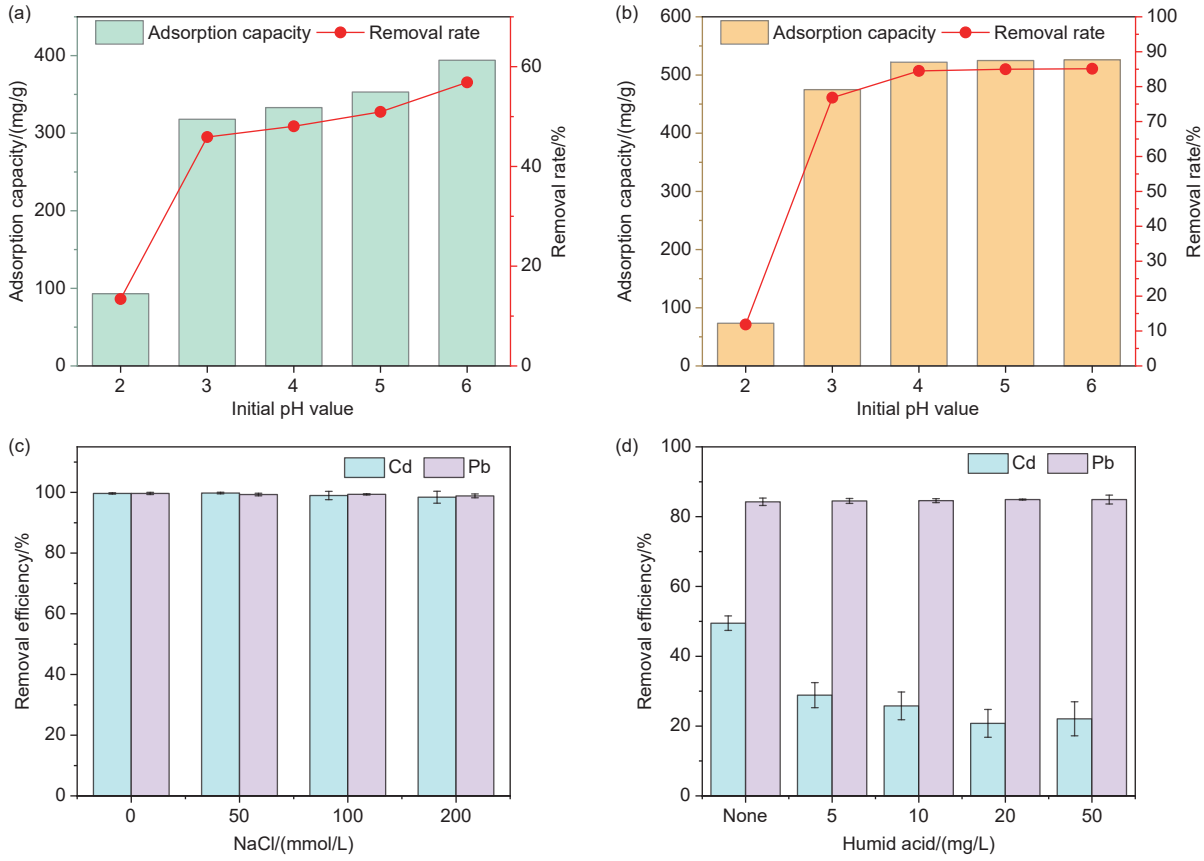

Fig. 6 (a) Effect of pH value on Cd(II) in MBC-700 adsorption solution. (b) Effect of pH on Pb(II) in MBC-700 adsorption solution. (c) Effect of ionic strength. (d) Humic acid concentration on Cd(II) and Pb(II) in MBC-700 adsorption solution. (Adsorbent dose=1 g/L, pH = 5.0 ± 0.1, C_0 = 100 mg/L for both metals in the ionic strength experiments and C_0 = 600 mg/L for the other experiments.)

adapted to aquatic environments with different salt contents, and the adsorption process is consistent with the inner-sphere complexation mechanism[52−53].

3.3.3 Effect of Humid acid

The effect of Humid acid (HA) on the adsorptive removal of Cd(II) and Pb(II) by MBC-700 is shown in Fig. 6d. The presence of HA slightly increases the removal of Pb(II) from water by MBC-700, and increased complexation and electrostatic attraction may be responsible for the higher removal rate. In contrast, the removal of Cd(II) by MBC-700 decreases as the concentration of HA becomes larger, which may be due to the fact that during the adsorption of Cd(II) by MBC-700, HA not only competes with MBC-700, but also shields some of the adsorption sites on MBC-700[54]. For Cd(II), its relatively weaker binding with HA makes competitive adsorption and steric shielding effects more pronounced.

3.4 Adsorption mechanisms

The experimental results showed that the adsorption of Cd(II) and Pb(II) by MBC-700 proceeds mainly by chemisorption. Ion exchange, electrostatic attraction, precipitation and surface complexation are the possible adsorption mechanisms (Fig. 7). Therefore, the adsorption mechanism was discussed in detail.

3.4.1 Ion exchange

MBC-700 is rich in exchangeable Mg^{2+}, which promotes the removal of Cd(II) and Pb(II) from wastewater. After adsorbing Cd(II) and Pb(II), the Mg content of MBC-700 decreases from 2.2% to 0.5% and 0.2%, respectively (Fig. S2, Fig. S5a-b). These results confirm that part of Mg^{2+} is partially exchanged during the adsorption process, indicating the occurrence of ion exchange between MBC-700 and Cd(II)/Pb(II).

3.4.2 Electrostatic attraction

The heavy metal ions present in the aqueous solution are often divalent or greater than divalent cations, and the deprotonation process of the functional groups on the adsorbent surface can lead to a negative charge on the adsorbent surface, and the opposite charges of the two may promote the migration rate of cations to the surface of the negatively charged adsorbent[55]. As shown in Fig. S4, the point of zero charge (pH_{pzc}) of MBC-700 is ~ 2.47. When pH < pH_{pzc}, the surface of MBC-700 is more positively charged, and MBC-700 will electrostatically repel the heavy metal cations in solution. But at pH > pH_{pzc}, the MBC-700 becomes more negative as the pH increases. The lower zeta potential is more likely to be more effective in the adsorption of MBC-700 with heavy metal ions Cd(II) and Pb(II). The negative charge on the surface of MBC-700 exerts an electrostatic attraction toward Cd(II) and Pb(II) cations, serving as the initial driving force. Once ions are drawn close to the surface, short-range mechanisms (such as surface complexation, ion exchange, or pre-

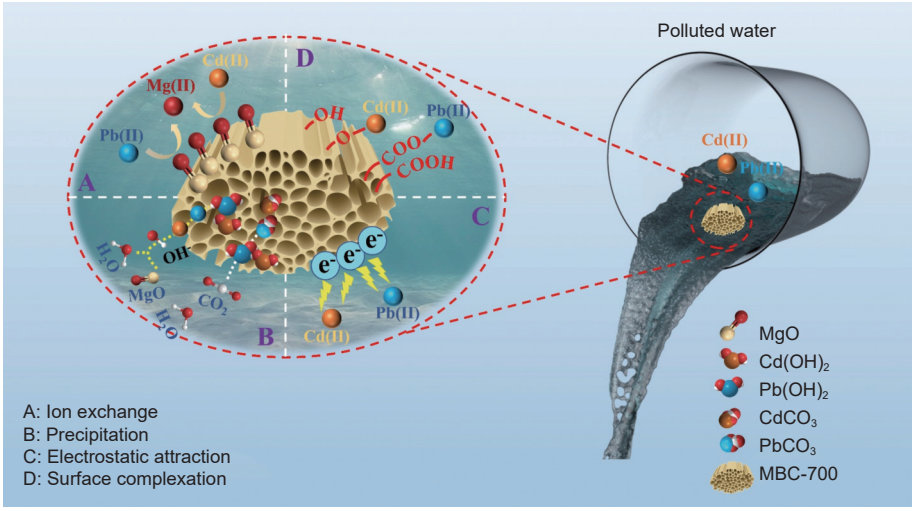

Fig. 7 Adsorption mechanism of Cd(II) and Pb(II) by MBC-700

cipitation) and the pervasive van der Waals forces collectively ensure the robust immobilization of ions[56]. Therefore, electrostatic attraction plays an important role in the adsorption of Cd(II) and Pb(II).

3.4.3 Precipitation

SEM was used to characterize the morphology of adsorbed MBC-700 samples, and EDS was used to analyze the chemical composition of the adsorbed MBC-700 samples. The results are shown in Fig. 8. After the adsorption of Cd(II), a large number of white precipitates appeared on MBC-700 (Fig. 8a-c). In order to determine the elemental composition of these white precipitates, the chemical composition of the region in Fig. 8d was analyzed. The results show that these precipitates contained a large amount of Cd (Fig. 8g and Fig. S5a), which indicated that Cd(II) is adsorbed and immobilized on MBC-700 mainly in the form of compounds. The microscopic morphology of the Cd compounds is in the form of thin flakes (Fig. 8c), most of which were stacked together and distributed in the pores of MBC-700 (Fig. 8d and Fig. 8g), which could be attributed to the ion exchange between Cd(II) and MgO particles present in the pores, and then reacted to form a precipitate that is adsorbed and immobilized in the pores (Fig. 2g).

The XRD of MBC-700 after adsorption was further observed (Fig. 9a). Analysis of MBC-700 after Cd(II) adsorption shows that the diffraction peak corresponding to MgO vanishes. Meanwhile, new diffraction peaks appearing at 2θ values of 23.47°, 30.28°, 36.33°, 43.69° and 49.86° are identified as $CdCO_3$ (JCPDS 42-1342), which forms through the reaction between $Cd(OH)_2$ and aqueous CO_2[57].

The FT-IR of MBC-700 before and after adsorption is shown in Fig. 9b. Vibrational peaks corresponding to the Mg—O functional group vanish following adsorption. Meanwhile, the peaks observed at 684 and 857 cm^{-1} are assigned to Pb—O and Cd—O (for Pb(II) and Cd(II) adsorption respectively), a phenomenon presumably resulting from ion exchange

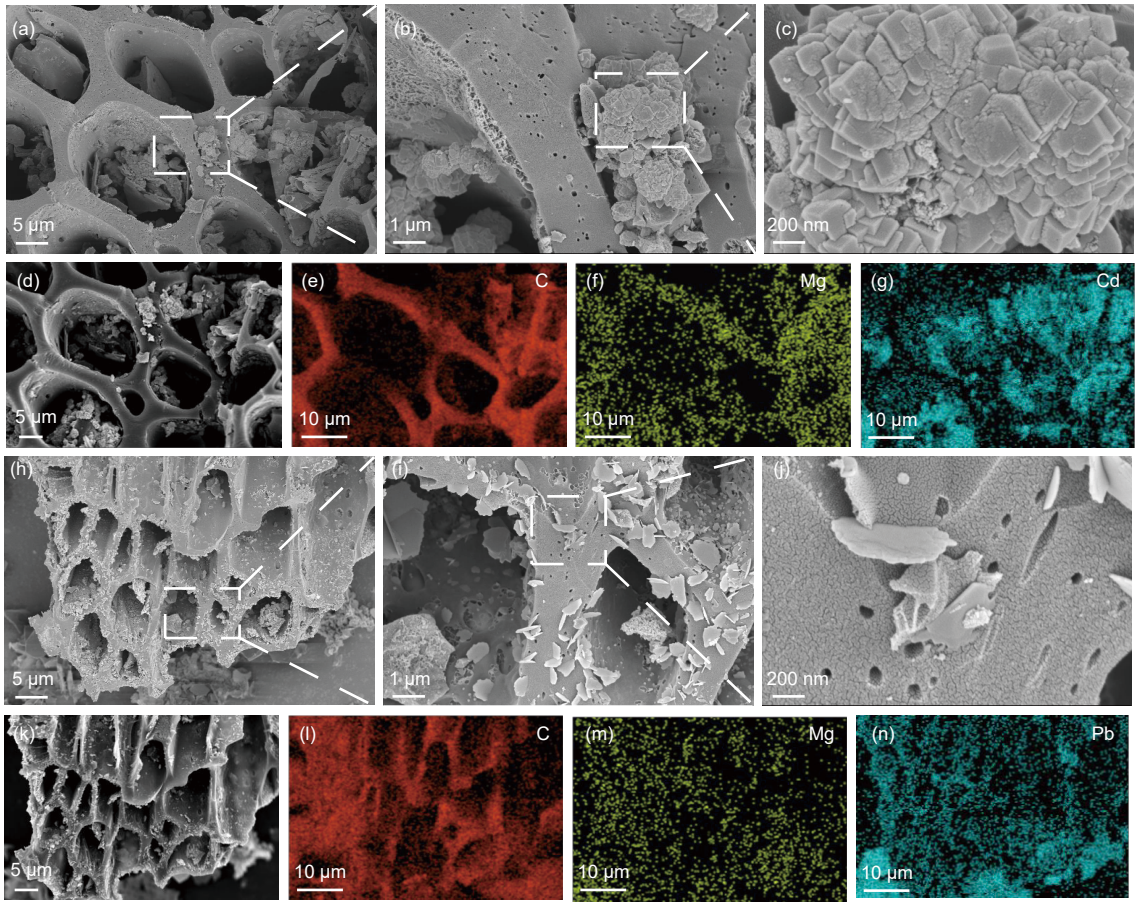

Fig. 8 (a-c) SEM and (d-g) EDS elemental mapping of MBC-700+Cd. (h-j) SEM and (k-n) EDS elemental mapping of MBC-700+Pb

during the adsorption process. Additionally, the strong vibrational peaks at 1415 and 1385 cm^{-1} are attributed to the stretching vibrations of CO_3^{2-}, which is derived from $CdCO_3$ and $PbCO_3$ formed in the adsorption reaction[58]. After MBC-700 adsorbs Cd(II) and Pb(II), its —OH vibrational peak (at ~ 3400 cm^{-1}) is notably weakened or even absent—this confirms the involvement of hydroxyl groups in the adsorption process[27].

Due to the large number of mesopores formed on the surface of MBC-700 through NaOH etching during the modification process, more adsorption sites were created. The SEM images in Fig. 8h-j and Fig. 10 show that the Pb compounds resulting from the adsorption of Pb(II) by MBC-700 were embedded on its surface.

The distribution of Cd and Pb compounds on MBC-700 confirms the validity of the multi-level porous MgO/biochar structure. Following Pb(II) adsorption, distinct new diffraction peaks appear at 2θ values of 19.95°, 20.97°, 24.65°, 27.06°, 34.21°, 40.40°, 42.61° and 44.10° in MBC-700's XRD pattern (Fig. 9a). These peaks are attributed to $Pb_3(CO_3)_2(OH)_2$ (JCPDS 13-0131), confirming that the lead-containing compound generated is basic lead carbonate[59].

In addition, the Pb 4f and Cd 3d peaks are clearly observed in the XPS full spectrum of MBC-700 after adsorption of Cd(II) and Pb(II) (Fig. 11a).

3.4.4 Surface complexation

The XPS characterization of MBC-700 before and after Cd and Pb adsorption is shown in Fig. 11. There are 4 characteristic peaks in the C 1s spectrum of MBC-700 (Fig. 11b), including C—C (284.8 eV), C—O (286.03 eV), C=O (287.96 eV) and O=C—O (290.41 eV)[60]. After heavy metal adsorption, the binding energies of the 4 peaks exhibited minor variations. For instance, after adsorbing Cd(II) and Pb(II) the peak area of the O=C—O group on the adsorbent decreased by 4% and 2%, respectively, while the area of the C—O peak also declined —this observation suggests that both the O=C—O and C—O groups participate in the adsorption process. A comparable phenomenon is observed when comparing the O 1s spectra of MBC-700 before and after Cd(II) or Pb(II)

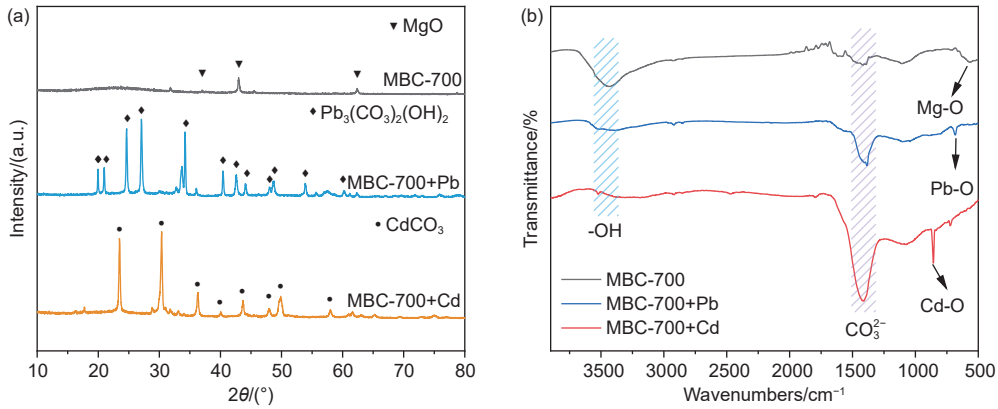

Fig. 9 (a) XRD patterns and (b) FT-IR spectra of MBC-700 before and after adsorption

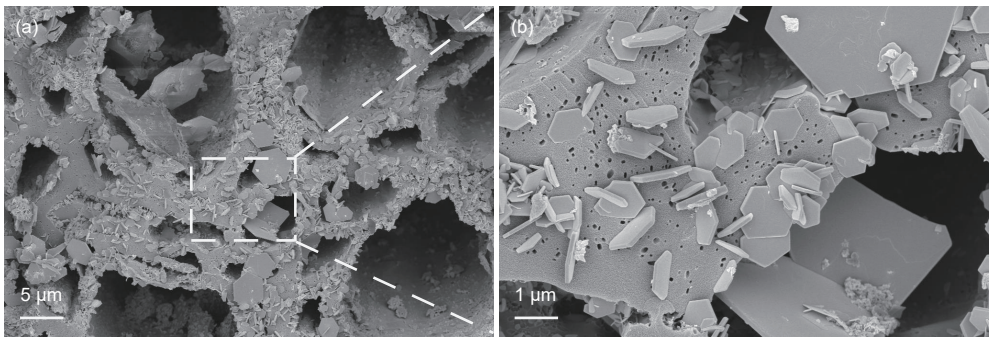

Fig. 10 (a-b) SEM images of MBC-700+Pb

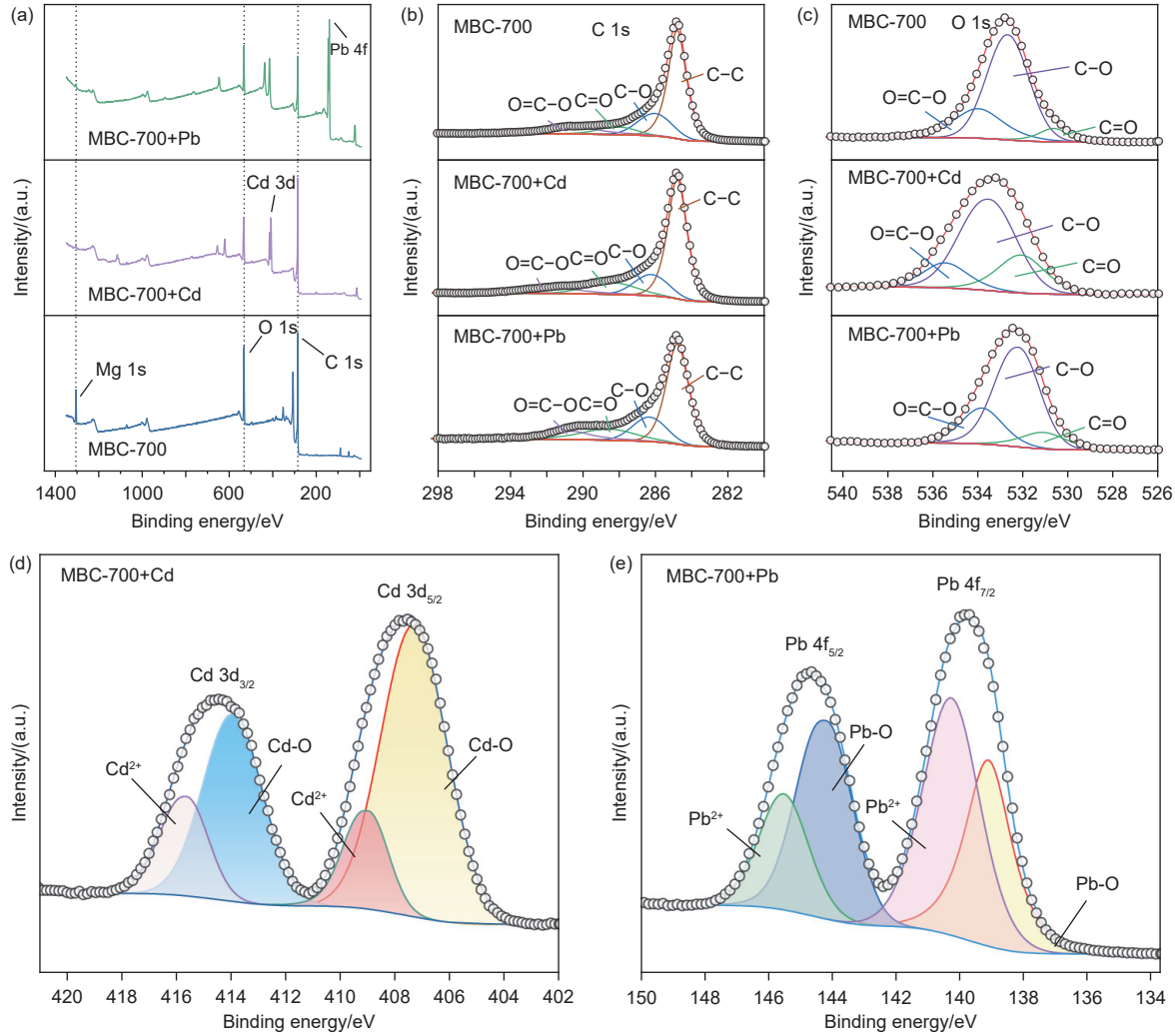

Fig. 11 XPS of MBC-700 before and after adsorption of Cd(II) and Pb(II). (a) Full XPS spectrum and spectrograms of (b) C 1s, (c) O 1s, (d) Cd 3d, and (e) Pb 4f

adsorption (Fig. 11c). These results are consistent with the study reported by Wu et al[61].

As shown in Fig. 11d, two peaks can be observed in the spectrum of MBC-700+Cd, which attributed to Cd $3d_{3/2}$ and Cd $3d_{5/2}$, respectively. The two peaks in the spectrum of MBC-700+Pb can be assigned to Pb $4f_{5/2}$ and Pb $f_{7/2}$ (Fig. 11e). Cd^{2+} and Cd—O are the main forms of Cd(II) adsorption on the biochar surface, and for Pb(II) adsorption, mainly Pb^{2+} and Pb—O.

3.5 Lead and cadmium recovery

Phytoremediation and biosorption are the 2 most common methods of removing heavy metals from soil and water through biomass adsorption. The remediation of soil and groundwater contaminated with heavy metals using hyper-enriched plants has been implemented in certain provinces of China. However, phytoremediation produces a large amount of heavy metal-rich biomass, which is currently not handled properly. The common treatment method is to burn these heavy metal-rich biomasses into ash and then treat them as special waste to be landfilled or stored with other metal slags, a process that does not retrieve the heavy metals adsorbed in the biomasses for further applications. To address this drawback, in this research work, the reductive properties of biochar at high temperatures were employed to convert Pb compounds adsorbed on biochar to the metallic Pb. The specific experimental steps were as follows: MBC-700+Pb after adsorption of Pb(II) was collected, placed in a tube furnace, heated to 800 °C in an N_2 environment and kept at this temperature for 2 h.

The XRD and XPS characterization of the reduction products are shown in Fig. 12. As can be seen in Fig. 12a, a peak for metallic lead can be clearly observed for the reduction product, corresponding to the standard card PDF#97-064-8341, and a diffraction peak for PbO was also detected, probably because the reduction reaction was not carried out thoroughly. Furthermore, the characteristic peaks of metallic lead were observed in the XPS of the reduction products (Fig. 12b), located at 142.1 and 137.0 eV, which further corroborated the success of the experiment in recovering metallic lead[62].

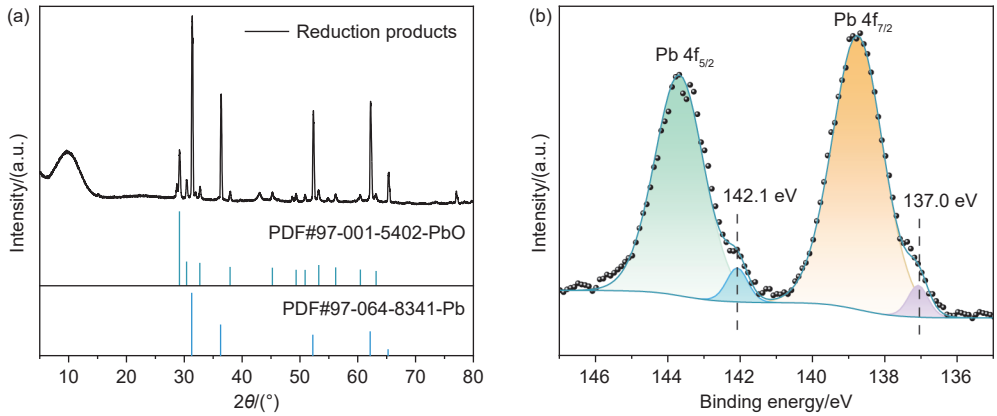

Fig. 12 (a) XRD patterns and (b) XPS spectra of reduction products

Nevertheless, when the same experimental procedure was employed for the recovery of Cd, the results did not yield metallic Cd (Fig. S6). This phenomenon may be attributed to the fact that the melting and boiling points of Cd are lower than 800 °C. When the temperature is maintained at 800 °C, the metallic Cd in the reduction product is converted to a gas. Subsequent attempts to collect metallic Cd can be made by connecting a condenser tube to the outlet of the tube furnace.

4 Conclusions

MBC samples with multi-level pore structure were prepared by co-impregnation method using lavender straw as the raw material and template. After the co-impregnation treatment, not only was the natural orderly tubular structure of lavender straw retained, but also multi-level porous structures were produced loaded with MgO nanoparticles. The specific surface area increased from 3 m^2/g of the BC to 158 m^2/g of MBC-700. Meanwhile, the multi-level pore structure and MgO nanoparticles loaded on the multi-level pore structure of MBC-700 enhanced the ion exchange capacity of MBC-700 by increasing the alkali metal ion (Mg^{2+}) content, endowing MBC-700 with high adsorption capacity for Pb(II) and Cd(II). Adsorption kinetics experiments showed that MBC-700 exhibited adsorption capacities of up to 520 mg/g for Cd(II) and 781 mg/g for Pb(II), which are 7–8 times greater than those of BC. Adsorption isotherm experiments revealed that the actual maximum adsorption capacities of MBC-700 reached 808 mg/g for Pb(II) and 520 mg/g for Cd(II). In addition, MBC-700 has good pH adaptability and resistance to ionic interference. Finally, metallic lead was successfully recovered using the reducing properties of biochar at high temperatures. This work not only effectively removes Cd(II) and Pb(II) in wastewater, but also solves the potential pollution resulting from inappropriate landfill treatment of crop straw on water sources.

Acknowledgements

This research was funded by the National Natural Science Foundation of China (52563033), Xinjiang Natural Science Fund for Distinguished Young Scholars (2022D01E37), Xinjiang Tianshan Talent Project (2024TSYCCX0007), and Key programs of Xinjiang Natural Science Foundation (2022B02051, 2023B2045 and 2024LQ01001-3).

References

[1] Wang J, Wang P, Wang H, et al. Preparation of molybdenum disulfide coated Mg/Al layered double hydroxide composites for efficient removal of chromium (VI)[J]. ACS Sustainable Chemistry & Engineering, 2017, 5(8): 7165-7174.

[2] Qiu B, Tao X, Wang H, et al. Biochar as a low-cost adsorbent for aqueous heavy metal removal: A review[J]. Journal of Analytical and Applied Pyrolysis, 2021, 155.

[3] Cheng B, Wang Z, Yan X, et al. Characteristics and pollution risks of Cu, Ni, Cd, Pb, Hg and As in farmland soil near coal mines[J]. Soil & Environmental Health, 2023, 1(3): 100035.

[4] Zhuang P, Chen F, Chen X, et al. The influence of food on in vivo Cd and Pb relative bioavailability in rice[J]. Food Chemistry Advances, 2023, 2: 100302.

[5] Mia S, Dijkstra F A, Singh B. Aging induced changes in biochar's functionality and adsorption behavior for phosphate and ammonium[J]. Environmental Science & Technology, 2017, 51(15): 8359-8367.

[6] Shahrokhi-Shahraki R, Benally C, El-Din M G, et al. High efficiency removal of heavy metals using tire-derived activated carbon vs commercial activated carbon: Insights into the adsorption mechanisms[J]. Chemosphere, 2021, 264: 128455.

[7] Shen C, Chen C, Wen T, et al. Superior adsorption capacity of g-C3N4 for heavy metal ions from aqueous solutions[J]. Journal of Colloid and Interface Science, 2015, 456: 7-14.

[8] Fayyazi F, Fatmehsari Haghshenas D, Kowsari E, et al. Synthesis of a three-dimensional reduced graphene oxide aerogel decorated with (Fe_3O_4@SiO_2–NH_2)–COC_2H_4COOH for adsorption of heavy metal cations[J]. Journal of Molecular Liquids, 2023, 386: 122512.

[9] Fan Q, Sun J, Chu L, et al. Effects of chemical oxidation on surface oxygen-containing functional groups and adsorption behavior of biochar[J]. Chemosphere, 2018, 207: 33-40.

[10] Hu R, Xiao J, Wang T, et al. Highly concentrated amino-modified biochars using a plasma: Evolution of surface composition and porosity for heavy metal capture[J]. Carbon, 2020, 168: 515-527.

[11] Sizmur T, Fresno T, Akgül G, et al. Biochar modification to enhance sorption of inorganics from water[J]. Bioresource Technology, 2017, 246: 34-47.

[12] Lyu H, Gao B, He F, et al. Effects of ball milling on the physicochemical and sorptive properties of biochar: Experimental observations and governing mechanisms[J]. Environ Pollut, 2018, 233: 54-63.

[13] Garg S, Goel N. Encapsulation of heavy metal ions via adsorption using cellulose/ZnO composite: First principles approach[J]. Journal of Molecular Graphics and Modelling, 2023, 124: 108566.

[14] Cheng S, Meng W, Xing B, et al. Efficient removal of heavy metals from aqueous solutions by Mg/Fe bimetallic oxide-modified biochar: Experiments and DFT investigations[J]. Journal of Cleaner Production, 2023, 403: 136821.

[15] Qu J, Che N, Niu G, et al. Iron/manganese binary metal oxide-biochar nano-composites with high adsorption capacities of Cd^{2+}: Preparation and adsorption mechanisms[J]. Journal of Water Process Engineering, 2023, 51: 103332.

[16] Ling L L, Liu W J, Zhang S, et al. Magnesium oxide embedded nitrogen self-doped biochar composites: Fast and high-efficiency adsorption of heavy metals in an aqueous solution[J]. Environmental Science & Technology, 2017, 51(17): 10081.

[17] Yang J, Wei Q, Tian C, et al. Preparation of biomass carbon composites MgO@ZnO@BC and Its Adsorption and Removal of Cu(II) and Pb(II) in wastewater[J/OL] 2023, 28(19): 6982.

[18] Wang Y, Wang L, Li Z, et al. MgO-laden biochar enhances the immobilization of Cd/Pb in aqueous solution and contaminated soil[J]. Biochar, 2021, 3(2): 175-188.

[19] Chen W, Feng J, Liu S, et al. A green and economical MgO/biochar composite for the removal of U(VI) from aqueous solutions[J]. Chemical Engineering Research and Design, 2022, 180: 391-401.

[20] Li Y, Liu Y, Liu C, et al. Quantitatively ion-exchange between Mg(II) and Pb(II)/Cd(II) during the highly efficient adsorption by MgO-loaded lotus stem biochar[J]. Journal of the Taiwan Institute of Chemical Engineers, 2023, 144.

[21] Sun M, Ma Y, Yang Y, et al. Effect of iron impregnation ratio on the properties and adsorption of KOH activated biochar for removal of tetracycline and heavy metals[J]. Bioresource Technology, 2023, 380: 129081.

[22] Qu J, Wang Y, Tian X, et al. KOH-activated porous biochar with high specific surface area for adsorptive removal of chromium (VI) and naphthalene from water: Affecting factors, mechanisms and reusability exploration[J]. Journal of Hazardous Materials, 2021, 401: 123292.

[23] Mu Y, He W, Ma H. Enhanced adsorption of tetracycline by the modified tea-based biochar with the developed mesoporous and surface alkalinity[J]. Bioresource Technology, 2021, 342: 126001.

[24] Hou Q, Rehman M L U, Bai X, et al. Incorporation of MgO into nitrogen-doped carbon to regulate adsorption for near-equilibrium isomerization of glucose into fructose in water[J]. Applied Catalysis B: Environmental, 2024, 342.

[25] Sahoo S K, Panigrahi G K, Dhal J P, et al. Co-axial electrospun hollow MgO nanofibers for efficient removal of fluoride ions from water[J]. Colloids and Surfaces A: Physicochemical and Engineering Aspects, 2022, 652.

[26] Tao X, Xu H, Luo S, et al. Construction of N-doped carbon nanotube encapsulated active nanoparticles in hierarchically porous carbonized wood frameworks to boost the oxygen evolution reaction[J]. Applied Catalysis B: Environmental, 2020, 279.

[27] Wu J, Wang T, Wang J, et al. A novel modified method for the efficient removal of Pb and Cd from wastewater by biochar: Enhanced the ion exchange and precipitation capacity[J]. Science of The Total Environment, 2021, 754: 142150.

[28] Zhang L, Fan J, Qian K, et al. Enhanced near-infrared transmission of ZnO-doped Y_2O_3-MgO nanocomposites with reduced light scattering due to decreased refractive index difference[J]. Journal of the European Ceramic Society, 2022, 42(11): 4616-4622.

[29] Chen B, Zhou D, Zhu L. Transitional adsorption and partition of nonpolar and polar aromatic contaminants by biochars of pine needles with different pyrolytic temperatures[J]. Environmental Science & Technology, 2008, 42(14): 5137-5143.

[30] Li H, Dong X, da Silva E B, et al. Mechanisms of metal sorption by biochars: Biochar characteristics and modifications[J]. Chemosphere, 2017, 178: 466-478.

[31] Biswas S, Rahaman T, Gupta P, et al. Cellulose and lignin profiling in seven, economically important bamboo species of India by anatomical, biochemical, FTIR spectroscopy and thermogravimetric analysis[J]. Biomass and Bioenergy, 2022, 158: 106362.

[32] Li B, Yang L, Wang C Q, et al. Adsorption of Cd(II) from aqueous solutions by rape straw biochar derived from different modification processes[J]. Chemosphere, 2017, 175: 332-340.

[33] Wang Y Y, Wang X Q, Li Y Q, et al. High-performance bamboo steel derived from natural bamboo[J]. ACS Applied Materials & Interfaces, 2021, 13(1): 1431-1440.

[34] Qi X, Yin H, Zhu M, et al. MgO-loaded nitrogen and phosphorus self-doped biochar: High-efficient adsorption of aquatic Cu^{2+}, Cd^{2+}, and Pb^{2+} and its remediation efficiency on heavy metal contaminated soil[J]. Chemosphere, 2022, 294: 133733.

[35] Wang Z, Nie E, Li J, et al. Carbons prepared from Spartina alterniflora and its anaerobically digested residue by H_3PO_4 activation: Characterization and adsorption of cadmium from aqueous solutions[J]. Journal of Hazardous Materials, 2011, 188(1): 29-36.

[36] Zhang D, Zhang K, Hu X, et al. Cadmium removal by $MgCl_2$ modified biochar derived from crayfish shell waste: Batch adsorption, response surface analysis and fixed bed filtration[J]. Journal of Hazardous Materials, 2021, 408: 124860.

[37] Wang H, Wang X, Teng H, et al. Purification mechanism of city tail water by constructed wetland substrate with NaOH-modified corn straw biochar[J]. Ecotoxicology and Environmental Safety, 2022, 238.

[38] Zhang M, Gao B, Yao Y, et al. Synthesis of porous MgO-biochar nanocomposites for removal of phosphate and nitrate from aqueous solutions[J]. Chemical Engineering Journal, 2012, 210: 26-32.

[39] Kushwaha R, Singh R S, Mohan D. Comparative study for sorption of arsenic on peanut shell biochar and modified peanut shell biochar[J]. Bioresource Technology, 2023, 375: 128831.

[40] Cai G, Ye Z L. Concentration-dependent adsorption behaviors and mechanisms for ammonium and phosphate removal by optimized Mg-impregnated biochar[J]. Journal of Cleaner Production, 2022, 349: 131453.

[41] Mubarak A S, Salih S S, Kadhom M, et al. Competitive and non-competitive adsorption of Cd(II) and Pb(II) from aqueous solution using Zr-BADS metal organic frameworks[J]. Sustainable Chemistry for the Environment, 2025, 9: 100231.

[42] Qi G, Pan Z, Zhang X, et al. Novel pretreatment with hydrogen peroxide enhanced microwave biochar for heavy metals adsorption: Characterization and adsorption performance[J]. Chemosphere, 2023: 140580.

[43] Yin G, Chen X, Sarkar B, et al. Co-adsorption mechanisms of Cd(II) and As(III) by an Fe-Mn binary oxide biochar in aqueous solution[J]. Chemical Engineering Journal, 2023, 466: 143199.

[44] Wang H, Chen Q, Xia H, et al. Enhanced complexation and electrostatic attraction through fabrication of amino- or hydroxyl-functionalized Fe/Ni-biochar composite for the adsorption of Pb(II) and Cd(II)[J]. Separation and Purification Technology, 2024, 328: 125074.

[45] Yan Y, Qi F, Zhang L, et al. Enhanced Cd adsorption by red mud modified bean-worm skin biochars in weakly alkali environment[J]. Separation and Purification Technology, 2022, 297: 121533.

[46] Liu X, Li D, Li J, et al. A novel MnO_x-impregnated on peanut shells derived biochar for high adsorption performance of Pb(II) and Cd(II): Behavior and mechanism[J]. Surfaces and Interfaces, 2022, 34: 102323.

[47] Chen H, Yang X, Liu Y, et al. KOH modification effectively enhances the Cd and Pb adsorption performance of N-enriched biochar derived from waste chicken feathers[J]. Waste Management, 2021, 130: 82-92.

[48] Cui Z, Xu G, Ormeci B, et al. A novel magnetic sludge biochar was prepared by making full use of internal iron in sludge combining KMnO4-NaOH modification to enhance the adsorption of Pb (Ⅱ), Cu (Ⅱ) and Cd (Ⅱ)[J]. Environmental Research, 2023, 236: 116470.

[49] Xia H, Zhang Y, Chen Q, et al. Unraveling adsorption characteristics and removal mechanism of novel Zn/Fe-bimetal-loaded and starch-coated corn cobs biochar for Pb(II) and Cd(II) in wastewater[J]. Journal of Molecular Liquids, 2023, 391: 123375.

[50] Luo X, Yu L, Wang C, et al. Sorption of vanadium (V) onto natural soil colloids under various solution pH and ionic strength conditions[J]. Chemosphere, 2017, 169: 609-617.

[51] Wang D, Luo W, Zhu J, et al. Potential of removing Pb, Cd, and Cu from aqueous solutions using a novel modified ginkgo leaves biochar by simply one-step pyrolysis[J]. Biomass Conversion and Biorefinery, 2023, 13(9): 8277-8286.

[52] Goldberg S. Inconsistency in the triple layer model description of ionic strength dependent boron adsorption[J]. Journal of Colloid and Interface Science, 2005, 285(2): 509-517.

[53] Xiao J, Hu R, Chen G, et al. Facile synthesis of multifunctional bone biochar composites decorated with Fe/Mn oxide micro-nanoparticles: Physicochemical properties, heavy metals sorption behavior and mechanism[J]. Journal of Hazardous Materials, 2020, 399: 123067.

[54] Wang Q, Zhang Y, Chen H, et al. Effects of humic acids on the adsorption of Pb(II) ions onto biofilm-developed microplastics in aqueous ecosystems[J]. Science of The Total Environment, 2023, 882: 163466.

[55] Zhao H, Lang Y. Adsorption behaviors and mechanisms of florfenicol by magnetic functionalized biochar and reed biochar[J]. Journal of the Taiwan Institute of Chemical Engineers, 2018, 88: 152-160.

[56] Li A, Ge W, Liu L, et al. Synthesis and application of amine-functionalized $MgFe_2O_4$-biochar for the adsorption and immobilization of Cd(II) and Pb(II)[J]. Chemical Engineering Journal, 2022, 439: 135785.

[57] Zhang Z, Li Y, Zong Y, et al. Efficient removal of cadmium by salts modified-biochar: Performance assessment, theoretical calculation, and quantitative mechanism analysis[J]. Bioresource Technology, 2022, 361: 127717.

[58] Deng J, Liu Y, Liu S, et al. Competitive adsorption of Pb(II), Cd(II) and Cu(II) onto chitosan-pyromellitic dianhydride modified biochar[J]. Journal of Colloid and Interface Science, 2017, 506: 355-364.

[59] Zhang L, Zhu W, Zhang H, et al. Hydrothermal–thermal conversion synthesis of hierarchical porous MgO microrods as efficient adsorbents for lead(ii) and chromium(vi) removal[J]. RSC Advances, 2014, 4(58): 30542-30550.

[60] Wu J, Wang T, Zhang Y, et al. The distribution of Pb(II)/Cd(II) adsorption mechanisms on biochars from aqueous solution: Considering the increased oxygen functional groups by HCl treatment[J]. Bioresource Technology, 2019, 291: 121859.

[61] Wu J, Wang T, Shi N, et al. Hierarchically porous biochar templated by in situ formed ZnO for rapid Pb^{2+} and Cd^{2+} adsorption in wastewater: Experiment and molecular dynamics study[J]. Environmental Pollution, 2022, 302.

[62] Che J, Zhang W, Xia L, et al. A facile and environmentally friendly approach for lead recovery from lead sulfate residue via mechanochemical reduction: Phase transformation and reaction mechanism[J]. ACS Sustainable Chemistry & Engineering, 2021, 9(30): 10227-10239.